Dynamic behavior of valence-shell excitations of atomic neon studied by high-resolution inelastic x-ray scattering

L. F. Zhu,[1,*] W. Q. Xu,[1] K. Yang,[2,†] Z. Jiang,[2] X. Kang,[1] B. P. Xie,[3] D. L. Feng,[3] N. Hiraoka,[4] and K. D. Tsuei[4]

[1]*Hefei National Laboratory for Physical Sciences at Microscale, Department of Modern Physics, University of Science and Technology of China, Hefei, Anhui 230026, People's Republic of China*

[2]*Shanghai Institute of Applied Physics, Chinese Academy of Sciences, Shanghai 201204, People's Republic of China*

[3]*State Key Laboratory of Surface Physics, Department of Physics, and Advanced Materials Laboratory, Fudan University, Shanghai 200433, People's Republic of China*

[4]*National Synchrotron Radiation Research Center, Hsinchu 30076, Taiwan, Republic of China*

The high-resolution inelastic x-ray scattering has been applied to study the excitation mechanism of atomic neon. The different electric multipolar transitions of neon, i.e., the electric monopolar, dipolar, and quadrupolar ones, were clearly resolved, and their squared form factors were determined. It is found that for the monopolar and quadrupolar transitions the present inelastic x-ray scattering results are in agreement with the ones measured by high-energy electron scattering, while for the dipolar transition large discrepancies between the results measured by these two methods were observed. Such phenomena are well elucidated with the aid of the second-order Born approximation: Born amplitude of a transition near zero momentum transfer is the key factor which determines the behavior of the intramolecular multiple scattering in the high-energy electron scattering. It is revealed that the intramolecular multiple scattering in high-energy electron scattering must be considered for the dipole-allowed transition, while it is negligible for the dipole-forbidden ones.

The dynamic parameters of atoms or molecules with high accuracy, i.e., the benchmark data, are of crucial importance to test the theoretical models, calculational codes, as well as the wave functions of target. According to Bethe-Inokuti theory [1–4], the generalized oscillator strengths (GOSs), which are often measured by high-energy electron energy loss spectroscopy (EELS), are thought to be only determined by the target structure under the hypothesis that the first Born approximation (FBA) is satisfied [1–4]. For helium, Bethe-Inokuti theory is valid according to the experimental and theoretical investigations for more than 40 years [5–8]. However, for other atoms, the disagreements between the experimental results and theoretical calculations in the larger momentum transfer region were generally observed [9–15]. These disagreements are strange because the experimental data measured by different groups [10,15] with different methods are in good agreement, while the electronic correlation is considered carefully in the calculation of random phase approximation with exchange (RPAE) [12–14,16,17]. Such discrepancy puzzled experimentalists and theorists for several years. Furthermore, since the 1970s, the theoretical investigations on the moderate energy electron impact [18–24] suggested that the high-order Born term may explain the much higher values of experimental differential cross sections (DCSs) at the large scattering angles, which implies that the extensively used simple physical picture proposed by Bethe and Inokuti [1–3] may not be sufficient to describe the high-energy electron collision process, even for several keV collision energies. However, no direct experimental evidence to verify such hypothesis existed until recently, so this old and

important problem is reinvestigated by a novel experimental technique—inelastic x-ray scattering (IXS) [5,6,25,26], which is a weak probe and free from the high-order Born term [27,28]. The results of Bradley *et al.* [25] on nitrogen suggested that the high-order Born term, i.e., it is termed intramolecular multiple scattering in their work, has contributions to the DCS of high-energy electron impact at large scattering angles. However, several important questions have not been fully addressed yet. Such as, to what extent the influence of the high-order Born term is, and whether the influence is the same for all transitions with different electric multipolarities such as electric monopole, electric dipole, electric quadrupole, etc. In this Rapid Communication, using neon as a paradigm and the high-resolution inelastic x-ray scattering as a probe, we try to give some clues about this question.

The previous experiments mostly measured the dynamic parameters of the valence-shell excitations of neon by low-energy ($\leqslant 100$ eV) [29–32] or moderate-energy (300–500 eV) [33,34] electron impact. The only available experimental data by high-energy electron impact at 2.5 keV is the state-resolved GOS measurements [9], to the best of our knowledge. As for the theoretical investigations, the GOSs or DCSs of the valence-shell excitations of neon were calculated by the FBA [35], the distorted-wave Born approximation [36], the frist-order many-body theory [37], as well as the relativistic distorted-wave Born approximation [38,39]. Recently, the RPAE method, in which the electronic correlation is carefully considered, was used to calculate the dynamic parameters of the valence-shell excitations of neon [12–14,17]. However, the obvious differences between the RPAE calculations and the experimental data are still observed [9]. To solve the debate, we use a different experimental technique, i.e., the IXS, to investigate the excitation process of neon.

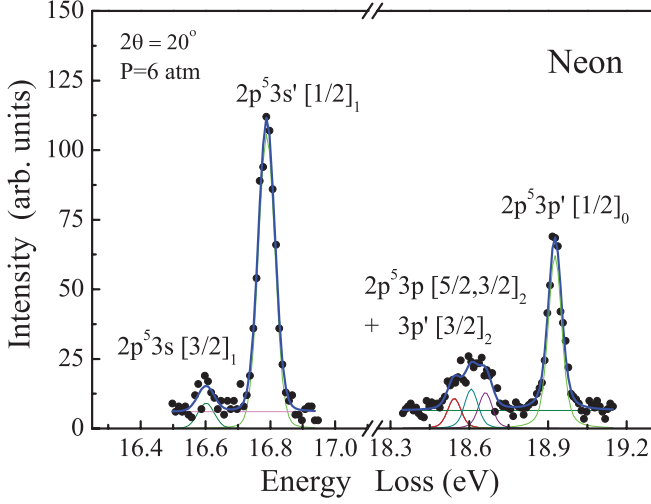*lfzhu@ustc.edu.cn.

†yangke@sinap.ac.cn

FIG. 1. (Color online) A typical inelastic x-ray scattering spectrum of neon gas.

The squared form factor $\zeta(q,\omega_n)$ of an electron and/or photon scattered by a target atom can be defined as (in atomic units) [6]

$$\zeta(\mathbf{q},\omega_n) = \left| \langle \Psi_n | \sum_{j=1}^{N} \exp(i\mathbf{q} \cdot \mathbf{r}_j) | \Psi_0 \rangle \right|^2$$

$$= \frac{1}{r_0^2} \frac{\omega_i}{\omega_f} \frac{1}{|\vec{\epsilon}_i \cdot \vec{\epsilon}_f^*|^2} \left(\frac{d\sigma}{d\Omega} \right)_\gamma, \quad (1)$$

$$= \frac{1}{4} \frac{k_i}{k_f} q^4 \left(\frac{d\sigma}{d\Omega} \right)_e = \frac{q^2}{2\omega_n} f(\mathbf{q},\omega_n), \quad (2)$$

where e,γ refer to electron and photon scattering, respectively. $d\sigma/d\Omega$ and $f(\mathbf{q},\omega_n)$ stand for the DCS and GOS, respectively. Ψ_0 and Ψ_n are the N-electron wave functions for the initial and final states, respectively. $\vec{\epsilon}_i$ and $\vec{\epsilon}_f$ stand for the polarization directions of the incident and scattered photons, respectively. The transferred momentum and energy from the incident electron or photon to the sample target are $\mathbf{q}(\mathbf{q} = \mathbf{k}_i - \mathbf{k}_f)$ and $\omega_n(\omega_n = \omega_i - \omega_f)$, respectively. $\mathbf{r}_j$ is the position vector of the jth electron, while r_0 is the classic electron radius.

The present IXS measurement of neon was carried out at the Taiwan Beamline BL12XU of SPring-8 with an energy resolution of 70 meV. The experimental setups and method used in this work were described in our previous works [5,6] in detail. In the present experiment, two different sample gases (neon and helium gases) with the same pressure of 6 atm were sealed in turn in a gas cell by Kapton window, then the gas cell was put on the experimental platform for the measurements in turn. The analyzer energy for the scattered photon was fixed at 9889.30 eV, while the incident photon energy varied, from which the energy loss was deduced. All the spectra of neon within the scattering angular range of 5°–55° and helium within the scattering angular range of 5°–20° were taken at room temperature. A typical inelastic x-ray scattering spectrum of neon is shown in Fig. 1, and the excited states are assigned. The intensity for the individual transition was determined by fitting the measured spectra. Then the previously calculated DCS of the $2\,^1P$ of helium [8] was
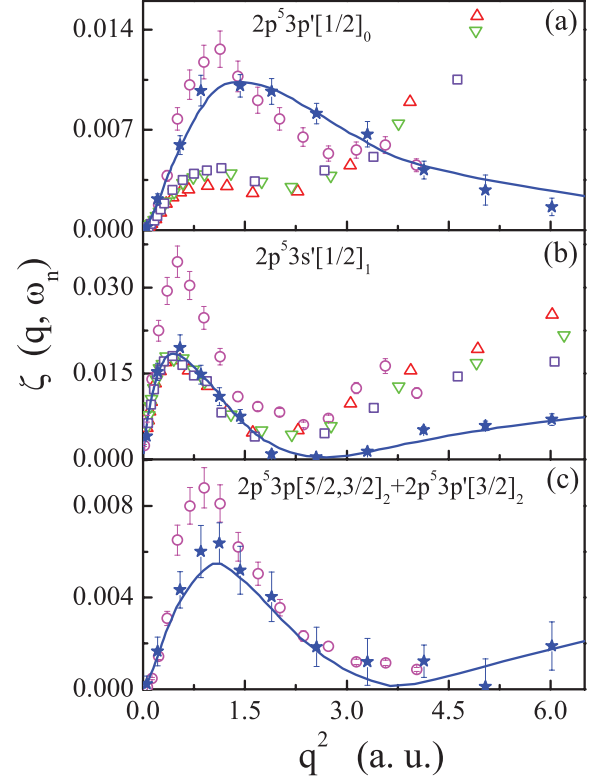

FIG. 2. (Color online) The squared form factors $\zeta(q,\omega_n)$ for the electric monopolar (a), dipolar (b), and quadrupolar (c) transitions of neon. Solid (blue) star: the present IXS results; open (pink) circle: the results of Cheng *et al.* [9] at the incident electron energy of 2.5 keV; solid (navy blue) line: the RPAE calculations [17]. The (red) triangle, (green) down-triangle, and (violet) square are the results of Suzuki *et al.* [33] measured at the incident electron energies of 300, 400, and 500 eV, respectively.

used to calibrate the variable collision length in the scattering angular range of 5°–20° caused by the finite size of the gas cell and normalize the DCSs of the other excitations. The variable collision length in the scattering angular range of 25°–55° of neon was simply calibrated by a factor of $\sin(2\theta)$ as described in our previous paper [5]. From the measured intensities of the excitations of neon and $2\,^1P$ of helium at 20°, the squared form factor $\zeta(q,\omega_n)$ for the individual excitation of neon was normalized to the theoretical $\zeta(q,\omega_n)$ of the $2\,^1P$ of helium at 20° calculated by Han and Li [8], which is similar to the normalization method used in our previous paper [6]. The experimental errors of $\zeta(q,\omega_n)$ are attributed to the statistics of counts, the normalizing procedure, as well as the fitting procedure, which are shown in the corresponding figures.

The squared form factors $\zeta(q,\omega_n)$ for the electric monopolar transition of $2p^5 3p'[1/2]_0$, dipolar transition of $2p^5 3s'[1/2]_1$, and the quadrupolar transitions of $2p^5 3p[5/2,3/2]_2 + 2p^5 3p'[3/2]_2$ of atomic neon measured by the present IXS are shown in Fig. 2 along with the EELS measurements [9,33] and theoretical calculations [17]. The $\zeta(q,\omega_n)$ of EELS was converted from the corresponding GOSs by Eq. (2). Since Amusia *et al.* [17] only calculated the total $\zeta(q,\omega_n)$ for the dipolar transition of $2p^5 3s$, the theoretical data of RPAE shown in Fig. 2 (b) were obtained by multiplying the total $\zeta(q,\omega_n)$

with the square of the intermediate coupling coefficient of the singlet $^1P_1$ component of $2p^53s'[1/2]_1$ [9]. It can be seen from Fig. 2 that the present $\zeta(q,\omega_n)$ of IXS for all electric multipolar transitions is in excellent agreement with the calculations of RPAE except that a few data points are slightly out of the experimental errors. However, the results are different when the present results of IXS are compared with the data of EELS. For the electric monopolar and quadrupolar transitions, the data of EELS measured at an impact energy of 2.5 keV [9] generally agree with the results of IXS within the experimental uncertainties as shown in Fig. 2(a) and 2(c). As for the much lower values of EELS ones measured at 300–500 eV [33] shown in Fig. 2(a), it is because the FBA is not satisfied at these collision energies. For the electric dipolar transition shown in Fig. 2(b), the results of EELS measured at 2.5 keV [9] are much higher than the present ones of IXS except the data in the low-q^2 region. The similar phenomenon can be observed for the moderate collision energies [34], and the agreement between the $\zeta(q,\omega_n)$ of EELS at 300–500 eV [33] and the ones of IXS in 0–1.6 a.u. will be discussed later. According to the work of Bradley *et al.* [25], the much higher values of EELS data at high q^2 in Fig. 2(b) can be attributed to the intramolecular multiple scattering, i.e., the contributions from the high-order Born terms. But the question is why the $\zeta(q,\omega_n)$ of EELS at 2.5 keV and the ones of IXS are in agreement for the electric monopolar and quadrupolar transitions. Is the contribution from the high-order Born terms not important for these dipole-forbidden transitions?

For the high-energy electron impact, the differential cross section $(d\sigma/d\Omega)_e$ is equal to $\frac{k_f}{k_i}|f_B|^2$, where f_B is the inelastic form factor [4], and it is equal to $f_{B1} + f_{B2}$ within the second-order Born approximation (SBA) [4]. Here f_{B1} and f_{B2} are the first- and second-order Born scattering amplitude, respectively. In the conventional framework of Bethe-Inokuti theory, the FBA is adopted and the contribution from f_{B2} is neglected. However, the previous investigation [25] shows that the intramolecular multiple scattering, i.e., f_{B2}, has important contributions even for the high-energy electron impact. According to the work of Carvalho [22,24], f_{B2} can be written as

$$f_{B2} = -\sum_e \lim_{\epsilon \to 0^+} \frac{2}{\pi^2}$$
$$\times \int d\vec{k} \frac{[F_{ne}(\vec{k} - \vec{k}_f) - Z\delta_{ne}][F_{e0}(\vec{k}_i - \vec{k}) - Z\delta_{e0}]}{|\vec{k}_i - \vec{k}|^2 |\vec{k} - \vec{k}_f|^2 (k_e^2 - k^2 + i\epsilon)},$$
(3)

$$F_{\beta\alpha}(\vec{Q}) = \sum_{j=1}^Z \int \Psi_\beta^* \exp(i\vec{Q} \cdot \vec{r}_j) \Psi_\alpha dr_1 \cdots dr_Z. \quad (4)$$

The physical picture of the second-order Born term is: an incident electron with a momentum $\vec{k}_i$ is scattered by a target atom at initial state $|0\rangle$ into an intermediate state $|e\rangle$, then the scattered electron with a momentum $\vec{k}$ is rescattered by the same target into the final state $|n\rangle$. The final momentum of the scattered electron is $\vec{k}_f$. The momentum transfers of the first and second scatterings are $\vec{k} - \vec{k}_i$ and $\vec{k}_f - \vec{k}$, respectively. The total momentum transfer is $\vec{q} = \vec{k}_f - \vec{k}_i$. $F_{\beta\alpha}(\vec{Q})$ is known as the Born amplitude of a transition from state α to state β
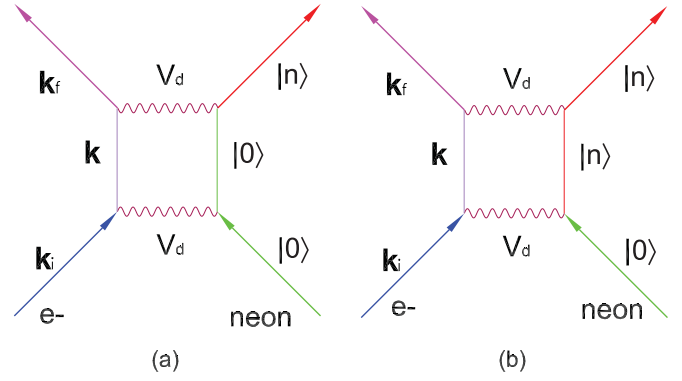

FIG. 3. (Color online) Sample Feynman diagrams of the dominant terms in f_{B2} for the inelastic transition $(\mathbf{k}_i, 0) \to (\mathbf{k}_f, n)$ of neon.

with a momentum transfer $\vec{Q}$ [22,24]. $k_e^2 = k_i^2 - 2w_e$, here w_e represents the excitation energy of the intermediate state $|e\rangle$ of target with atomic number Z. Other symbols have their common meanings. The summation in Eq. (3) is over all bound and continuum states, and δ_{ij} in Eq. (3) is the usual Kronecker symbol.

Although the summation in Eq. (3) is over all bound and continuum states, the dominant terms are that the intermediate state $|e\rangle$ is either the initial state $|0\rangle$ or the final state $|n\rangle$ as shown with Feynman diagrams in Fig. 3 since the DCS of the elastic scattering is much larger than that of the inelastic scattering. Figure 3(a) corresponds to the contribution to f_{B2} in which an elastic scattering from $|0\rangle$ to $|0\rangle$ is followed by an inelastic scattering from $|0\rangle$ to $|n\rangle$, while Fig. 3(b) represents the contribution in which the two steps reverse but the elastic scattering is from $|n\rangle$ to $|n\rangle$. It is apparent that the f_{B2} is dominated by the near zero value of the denominator in the right-hand side of Eq. (3), i.e., $\vec{k} \to \vec{k}_i$ or $\vec{k} \to \vec{k}_f$. According to the Feynman diagram in Fig. 3(a), $\vec{k} \to \vec{k}_i$ means that an elastic scattering at near zero momentum transfer ($\sim 0°$) is followed by an inelastic scattering at large momentum transfer (a large angle). However, compared with the direct inelastic scattering at a large angle, the second-order Born term f_{B2} at $\vec{k} \to \vec{k}_i$ shown in Fig. 3(a) should be much less, since it is a two-step process. In Fig. 3(a) $\vec{k} \to \vec{k}_f$ means that an elastic scattering at a large angle is followed by an inelastic scattering at a near zero angle. Since for high-energy electron impact the inelastic Born amplitude in Eq. (3) for the electric dipolar transition is concentrated at small angles, while the probability of elastic scattering decreases much slowly than the inelastic one as the scattering angle increases [4], the process of the elastic scattering at a large angle following by the inelastic scattering at a small angle ($\sim 0°$) dominates the second-order Born term f_{B2}. The similar discussion is valid for the Feynman diagram in Fig. 3(b), but the dominant contribution of f_{B2} is at $\vec{k} \to \vec{k}_i$ in which the inelastic scattering at a small angle from $|0\rangle$ to $|n\rangle$ is followed by the elastic scattering at a large angle from $|n\rangle$ to $|n\rangle$. Considering that the first-order Born amplitude for a dipolar transition at the large momentum transfer is very small, the above-mentioned f_{B2}, i.e., the elastic scattering at a large angle and the inelastic scattering at a very small angle, dominates the squared form factor of an electric dipolar transition for high-energy electron scattering in the

large momentum transfer region. This is the reason that the $\zeta(q,\omega_n)$ of EELS measured at the high-impact energy in the large-q^2 region is much larger than the present ones of IXS shown in Fig. 2(b). As for the agreement between the results of EELS at 300–500 eV [33] and the ones of IXS in the q^2 region of 0–1.6 a.u., it is reasonable because the momentum transfer at the angle of $0°$, which is inversely proportional to incident electron energy E_0, increases as the incident electron energy decreases [3]. The contribution from the f_{B2} at 300–500 eV is about five times smaller than that at 2.5 keV because of the large denominator in the right-hand side of Eq. (3), which leads to the agreement in the q^2 region of 0–1.6 a.u.

For a dipole-forbidden transition such as the electric monopolar or quadrupolar ones, its inelastic Born amplitude at near zero momentum transfer approaches to zero. Therefore, for the dominant contribution in Eq. (3) shown in Fig. 3(a) or 3(b), the elastic scattering at a large angle is followed by the inelastic scattering at a near-zero angle or the other way around, although $\vec{k} \to \vec{k}_i$ or $\vec{k} \to \vec{k}_f$ results in a near-zero denominator in Eq. (3), the near-zero numerator counteracts the influence. Therefore, compared with the large value of the Born amplitude of the direct inelastic scattering of the dipole-forbidden transition at large momentum transfer, the overall contribution to the f_{B2} is small, which explains the reasonable agreement between the present results of IXS and the ones of EELS measured at high impact energy [9] as shown in Fig. 2(a) and 2(c). Therefore, the intramolecular multiple scattering in high-energy electron collision is determined by the Born amplitude at near zero momentum transfer of a transition.

In summary, using the high-resolution inelastic x-ray scattering, the state-resolved squared form factors for the electric monopolar transition of $2p^53p'[1/2]_0$, dipolar tran-

sition of $2p^53s'[1/2]_1$, as well as the quadrupolar transitions of $2p^53p[5/2,3/2]_2 + 2p^53p'[3/2]_2$ of atomic neon were determined. It is found that the agreements between the present squared form factors of IXS for the dipole-forbidden transitions and the ones of EELS are much better than that of the dipole-allowed transition. Such phenomena are well elucidated by the second-order Born approximation: the two steps of an elastic scattering at a large angle and an inelastic scattering at a near zero angle dominate the SBA, and the transition probability at the near zero momentum transfer of a transition determines the dynamic behavior of the SBA. The intramolecular multiple scattering in high-energy EELS is important for the electric dipolar transition because of the forward peaking behavior of its DCS, while it is negligible for the dipole-forbidden ones because of its near zero transition probability at dipole limit. Therefore, the high-energy EELS is a powerful tool to investigate the structure of atoms or molecules for the dipole-forbidden transition, but the contributions from the second-order Born term significantly influence the dynamic behavior of the dipole-allowed transition. In addition, the present work clarifies the difference between the GOSs measured by high-energy electron impact experiments and the theoretical calculations [9–15].

[1] H. Bethe, Ann. Phys. (NY) **5**, 325 (1930).

[2] H. Bethe, Z. Phys. **76**, 293 (1930).

[3] M. Inokuti, Rev. Mod. Phys. **43**, 297 (1971).

[4] B. H. Bransden and C. J. Joachain, *Physics of Atoms and Molecules* (Prentice Hall, Harlow, UK, 2003).

[5] B. P. Xie, L. F. Zhu, K. Yang, B. Zhou, N. Hiraoka, Y. Q. Cai, Y. Yao, C. Q. Wu, E. L. Wang, and D. L. Feng, Phys. Rev. A **82**, 032501 (2010), and references therein.

[6] L. F. Zhu, L. S. Wang, B. P. Xie, K. Yang, N. Hiraoka, Y. Q. Cai, and D. L. Feng, J. Phys. B **44**, 025203 (2011), and references therein.

[7] X. J. Liu, L. F. Zhu, Z. S. Yuan, W. B. Li, H. D. Cheng, J. M. Sun, and K. Z. Xu, J. Electron Spectrosc. Relat. Phenom. **135**, 15 (2004).

[8] X. Y. Han and J. M. Li, Phys. Rev. A **74**, 062711 (2006).

[9] H. D. Cheng, L. F. Zhu, Z. S. Yuan, X. J. Liu, J. M. Sun, W. C. Jiang, and K. Z. Xu, Phys. Rev. A **72**, 012715 (2005).

[10] L. F. Zhu, H. D. Cheng, Z. S. Yuan, X. J. Liu, J. M. Sun, and K. Z. Xu, Phys. Rev. A **73**, 042703 (2006).

[11] W. B. Li, L. F. Zhu, X. J. Liu, Z. S. Yuan, J. M. Sun, H. D. Cheng, Z. P. Zhong, and K. Z. Xu, Phys. Rev. A **67**, 062708 (2003).

[12] M. Y. Amusia, L. V. Chernysheva, Z. Felfli, and A. Z. Msezane, Phys. Rev. A **67**, 022703 (2003).

[13] M. Y. Amusia, L. V. Chernysheva, Z. Felfli, and A. Z. Msezane, Phys. Rev. A **75**, 062703 (2007).

[14] Z. F. Chen and A. Z. Msezane, J. Phys. B **33**, 5397 (2000).

[15] X. W. Fan and K. T. Leung, Phys. Rev. A **62**, 062703 (2000).

[16] M. Y. Amusia, L. V. Chernysheva, Z. Felfli, and A. Z. Msezane, Phys. Rev. A **64**, 032711 (2001).

[17] M. Y. Amusia, L. V. Chernysheva, Z. Felfli, and A. Z. Msezane, Phys. Rev. A **65**, 062705 (2002).

[18] E. J. Kelsey, Phys. Rev. A **14**, 56 (1976).

[19] E. J. Kelsey, Ann. Phys. (NY) **322**, 1925 (2007).

[20] S. Geltman and M. B. Hidalgo, J. Phys. B **4**, 1299 (1971).

[21] C. B. Opal and E. C. Beaty, J. Phys. B **5**, 627 (1972).

[22] I. L. de Carvalho, J. Phys. B **26**, 2179 (1993).

[23] R. A. Bonham, J. Electron Spectrosc. Relat. Phenom. **3**, 85 (1974).

[24] I. L. de Carvalho, J. Phys. B **25**, 1287 (1992).

[25] J. A. Bradley, G. T. Seidler, G. Cooper, M. Vos, A. P. Hitchcock, A. P. Sorini, C. Schlimmer, and K. P. Nagle, Phys. Rev. Lett. **105**, 053202 (2010).

[26] J. A. Bradley, A. Sakko, G. T. Seidler, A. Rubio, M. Hakala, K. Hämäläinen, G. Cooper, A. P. Hitchcock, K. Schlimmer, and K. P. Nagle, Phys. Rev. A **84**, 022510 (2011).

[27] P. M. Platzman and N. Tzoar, Phys. Rev. **139**, A410 (1965).

[28] P. Eisenberger and P. M. Platzman, Phys. Rev. A **2**, 415 (1970).

[29] D. F. Register, S. Trajmar, G. Steffensen, and D. C. Cartwright, Phys. Rev. A **29**, 1793 (1984).

[30] M. A. Khakoo, T. Tran, D. Bordelon, and G. Csanak, Phys. Rev. A **45**, 219 (1992).

[31] M. A. Khakoo, C. E. Beckmann, S. Trajmar, and G. Csanak, J. Phys. B **27**, 3159 (1994).

[32] M. A. Khakoo, J. Wrkich, M. Larsen, G. Kleiban, I. Kanik, S. Trajmar, M. J. Brunger, P. J. O. Teubner, A. Crowe, C. J. Fontes *et al.*, Phys. Rev. A **65**, 062711 (2002).

[33] T. Y. Suzuki, H. Suzuki, S. Ohtani, B. S. Min, T. Takayanagi, and K. Wakiya, Phys. Rev. A **49**, 4578 (1994).

[34] T. Y. Suzuki, H. Suzuki, S. Ohtani, T. Takayanagi, and K. Okada, Phys. Rev. A **75**, 032705 (2007).

[35] P. S. Ganas and A. E. S. Green, Phys. Rev. A **4**, 182 (1971).

[36] T. Sawada, J. E. Purcell, and A. E. S. Green, Phys. Rev. A **4**, 193 (1971).

[37] L. E. Machado, E. P. Leal, and G. Csanak, Phys. Rev. A **29**, 1811 (1984).

[38] K. Bartschat and D. H. Madison, J. Phys. B **25**, 4619 (1992).

[39] M. Vos, R. P. McEachran, G. Cooper, and A. P. Hitchcock, Phys. Rev. A **83**, 022707 (2011).